Alondra Ortiz-Ortiz
Shuwei Zhang
Samuel Lee

Improving the sensitivity of high air flow-rate and flow-direction sensors

This paper reports an improvement in the sensitivity of high air flow-rate and flow-direction MEMS sensors. The need for flow-rate and flow-direction monitoring of air for different applications in the fields of environmental and meteorological monitoring is what motivates this engineering study. Highly sensitive flow-direction and flow-rate sensors can enhance the design of more efficient wind turbines (or more effectively using already existing wind turbines) and ultimately improving the production of environmentally friendly energy. These sensors could be used to **monitoring and predicting wind power and weather patterns** which is key for **a wide variety of processes** such as wind farm maintenance, optimal power flow between conventional units and wind farms, electricity marketing bidding, power system generators and energy storage planning and scheduling (El-Fouly, T.H.M. et al., 2008). The **current problem** with these sensors is the **lack of sensitivity at high flow-rates.** Certain designs such as the one described in Lee, C.Y. et al. (2009) are limited by mechanical stress limits and can only measure up to 35 m/s (mechanical failure occurs above 35 m/s). Other design are strictly only used for in-line pipe flow. With the integration of modern MEMS technology, the design and performance of these sensors could be improved.

Our design (**Figure 1**; fabrication process **Figure 2**) was based off of previous works by Kang, W. et al. (2018) and Lee, C.Y. et al. (2009). The design proposed by Lee, C. et al. (2009), an array of micro-cantilever sensors, have been proven to measure the flow-rate and flow direction but only at low-flow rates. The design of Kang, W. et al. (2018) utilized a heater-thermopile sensor that works with a wide range of flow-rate; however, this design cannot predict the direction of the flow. Hence, we combined the designs of these previous reports, the array and the heater-thermopile respectively, to measure both flow direction and speed in the in-plane. One portion of the array uses two thermopiles comprised of 37 pairs of thermocouples on opposite sides of a heater. When wind over the device pushes heat toward one thermopile, a measurable voltage difference is induced from the Seebeck effect. A circular pattern array of eight of these are used to measure flow-direction like the design of Lee, C.Y. et al (2009). Based on the direction of the wind, a particular heater-thermopile set will be more perpendicular to the flow and thereby resulting in a higher voltage difference. By comparing all the measurements of the array, direction can be determined. If more directional resolution is required, an array of more than eight could be used.

The design objectives included fitting the overall sensor in the footprint of the design proposed by Lee (a 20x20 mm area), having a sensitivity of at least 1 mV/(m/s), an estimated sensitivity shown by the experimental testing of the device in Kang, W. et al. (2018), without any electrical processing, and demonstrating capability at a wide range of wind speeds (at least up to 157 mph or 70 m/s, Hurricane Category 5 Wind Speeds). Overall, this study utilized SolidWorks™ to create models and COMSOL™ to evaluate and understand the effects of our design.

The first study (**Figure 3**) was a simplified flow field model to determine the effects of gap distances between the heater and the thermocouple as well as visualize the temperature contours at different wind speeds. We

determined that smaller gap distances were optimal for higher wind speeds and larger gaps were better for lower wind speeds. Next, a 2D simple thermoelectric model was created to demonstrate the thermoelectric effect on a single thermocouple (**Figure 4**). Then, we combined the 2D simple thermoelectric model and flowfield models and built a thermoelectric model (20 μm features) and a real model (200 nm features). We did a parameter sweeps on both the thermoelectric model and real model for a single thermocouple (**Figure 5** and **Figure 6**) to evaluate the device. The main study involved simulating the change in electric potential at different wind speeds. We found that the device could achieve the desired sensitivity, having an estimated sensitivity of at least 2 mV/(m/s) at 75 m/s but could be used at higher wind speeds. Lastly, we studied the effects of the device geometry and compared the performance of the device with 1 pair and 37 pairs of thermocouples. We observed that having more thermocouple pairs have an amplification effect of the signal, making it more sensitive. Future studies could be thermal stress analysis of the device, designing/studying the entire device (electrical circuit, signal processing, and packaging) including the dynamic response, and experimentally testing the device.

Our proposed design is proven to fit in the design area (**314.16 mm^2 total area**), maintain a high sensitivity (**about 2 mV/(m/s))**, and measure low and high wind speeds (up to **75m/s or 168 mph**). This design provides an opportunity to **improve environmental monitoring** by measuring speed and direction for **both low and high flow rates.** Our **high air flow-rate and flow-direction sensor** can be attached to the blades of wind turbines to determine their best location and orientation and to predict weather conditions. Ultimately, our design **advances MEMS technology** by developing **environmental friendly** and **low-cost high sensitivity sensors** while our fabrication process allows **mass production**.

Word Count: 886

References

COMSOL [Computer Software] (2015). How to Simulate Thermoelectric Devices and TECs. Retrieved from https://br.comsol.com/video/simulate-thermoelectric-devices-tecs

El-Fouly, T.H.M., El-Saadany, E. & Salama, M.M.A.. (2008). One Day Ahead Prediction of Wind Speed and Direction. *IEEE Transactions on Energy Conversion 23* (1), 191 - 201. 10.1109/TEC.2007.905069.

Kang, W., Choi, H. M., & Choi, Y. M. (2018). Development of MEMS-based thermal mass flow sensors for high sensitivity and wide flow rate range. *Journal of Mechanical Science and Technology*, *32*(9), 4237–4243. https://doi.org/10.1007/s12206-018-0822-4

Lee, C. Y., Wen, C. Y., Hou, H. H., Yang, R. J., Tsai, C. H., & Fu, L. M. (2009). Design and characterization of MEMS-based flow-rate and flow-direction microsensor. *Microfluidics and Nanofluidics*, *6*(3), 363–371. https://doi.org/10.1007/s10404-008-0381-6

Wang, Y. H., Lee, C. Y., & Chiang, C. M. (2007). A MEMS-based air flow sensor with a free-standing microcantilever structure. *Sensors*. https://doi.org/10.3390/s7102389

Appendix

1. Device CAD Model
2. Fabrication Process
3. Design Specifications and Materials Properties
4. Comsol Simulation and Analysis

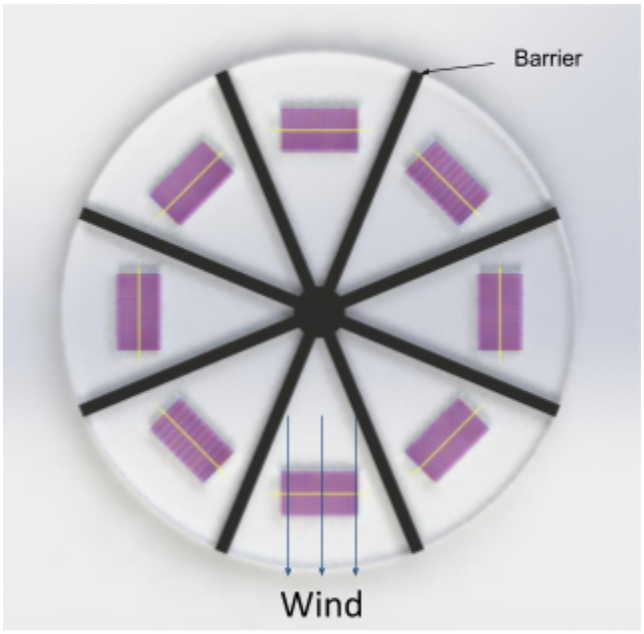

(a) Top

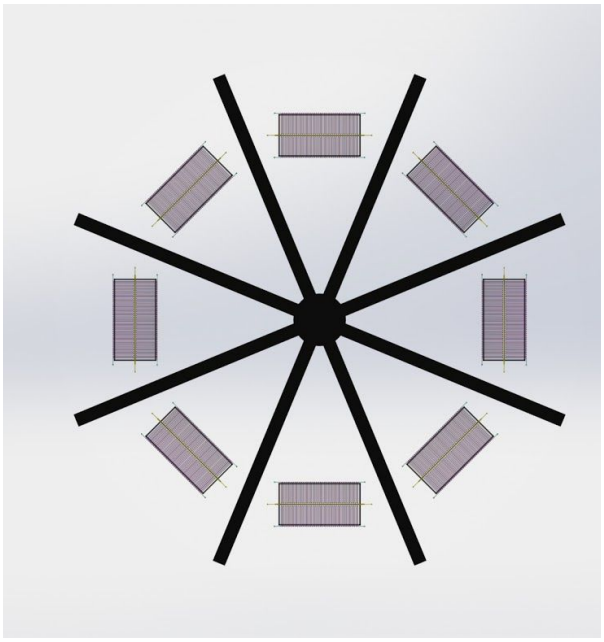

(b) Bottom

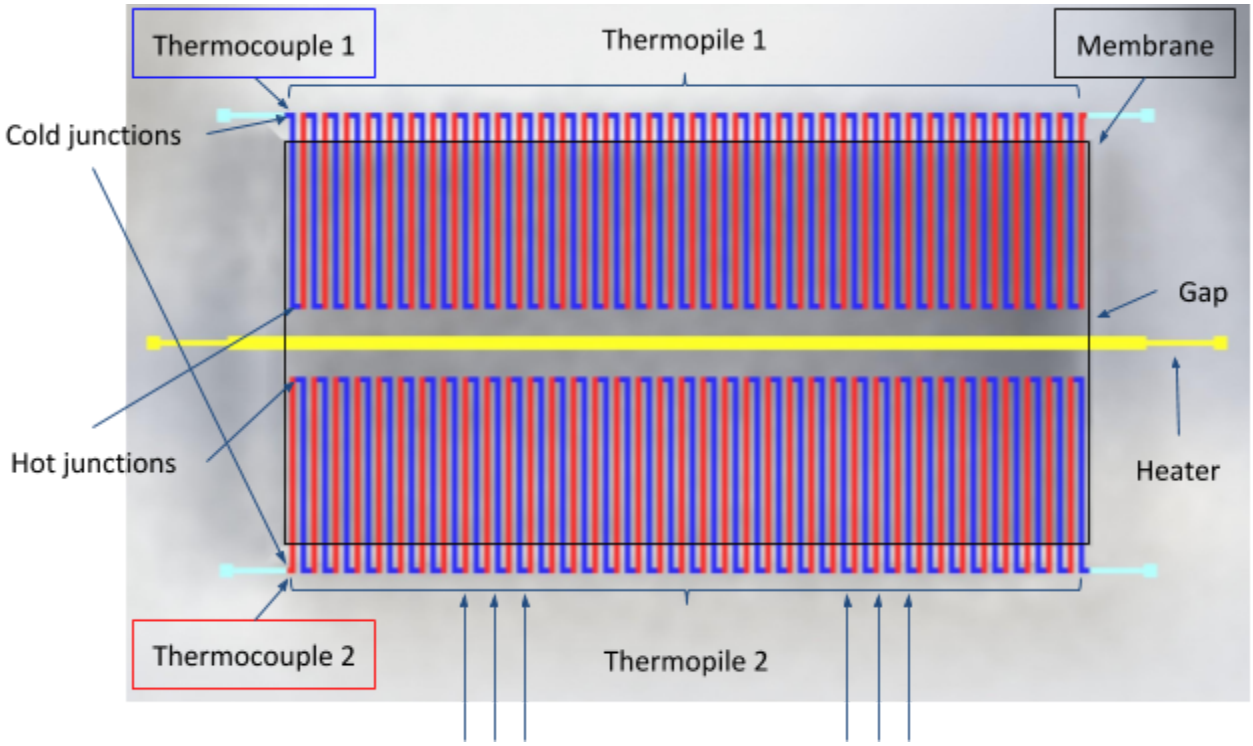

(c) Components of a single heater-thermopile

Figure 1. Proposed device solution of an array of heater-thermopile to measure flow direction and wind speed. The top of the device (a) shows a top view of the device. The bottom of the device (b) has a membrane. Each heater-thermopile portion of the device has several components (c): a heater that generates heat, a membrane to dissipate minimize conductive heat, two sets of thermopiles comprised of 37 pairs of thermocouples (red and blue represent the P and N type, respectively. When wind flows more perpendicularly over the sensor, the heat generated from the heater is moved to one thermopile, thereby inducing more of a voltage difference to that thermopile from the Seebeck effect.

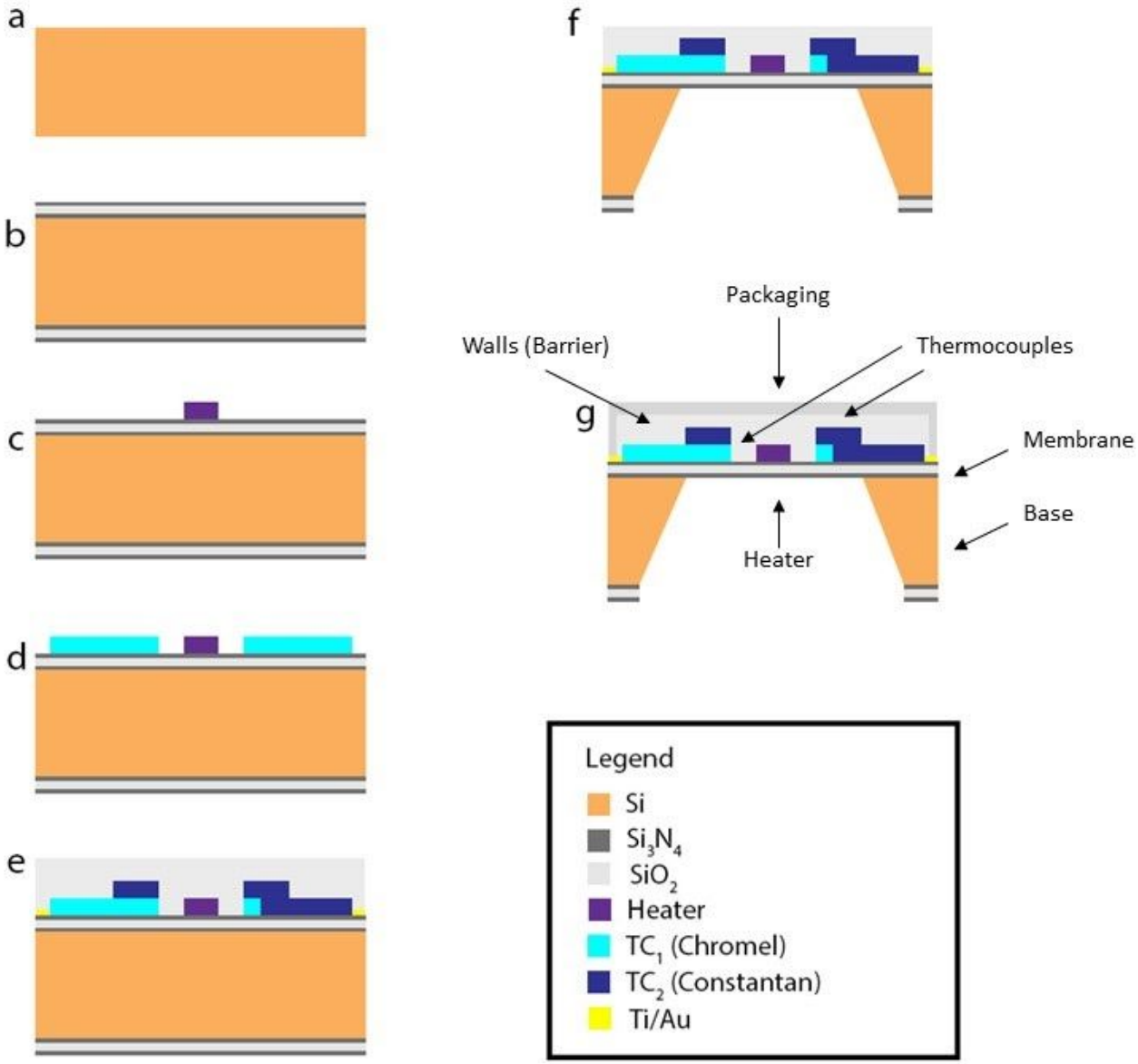

Figure 2. Fabrication process for the device: (a) The fabrication process starts with a 4-inch p-type silicon (Si) wafer. (b) A membrane of triple electric layers ($Si_3N_4/SiO_2/Si_3N_4$) is deposited using low pressure chemical vapor deposition (LPCVD) technique. A RF cleaning process is performed to remove the oxidation layer from the surface of the membrane. (c) The heater is patterned using a lift-off process and evaporated by E-beam sputtering. A photoresist is used as the mask for the lithography process. (d) E-beam sputtering is also used to evaporate the alloy thermopiles TC_1 and TC_2. Chrome is used as the seed layer between the membrane and the thermopiles. (e) 37 pairs of thermocouples are patterned. The barrier (SiO_2) is deposited using LPCVD. Contacts are sputtered on (Ti/Au). (f) Deep Reactive Ion Etching (DRIE) is conducted in the back side of the silicon wafer. (g) The device is wired and packaged. This fabrication process was adapted from Kang, W., Choi, H. M., & Choi, Y. M., 2018.

Table 1. Design specifications. All dimensions were obtained from SolidWorks.

Design Specifications				
Part	**Material**	**Dimensions**		
Base	**Si**	diameter: 20 mm		thickness: 0.5 mm
Walls	**SiO_2**	length: 9.0 mm	width: 0.5 mm	thickness: 0.002 mm
Membrane	**$Si_3N_4/SiO_2/Si_3N_4$**	length: 3.12 mm	width: 1.62 mm	thickness: 0.5 mm
Heater	**Evanohm R (Ni-Cr Alloy)**	length: 4.0 mm	width: 0.05 mm	thickness: 0.0002 mm
TC1	**Chromel (Ni-Cr Alloy)**	length: 0.725 mm	width: 0.03 mm	thickness: 0.0002 mm
TC 2	**Constantan (Cu-Ni Alloy)**	length: 0.725 mm	width: 0.03 mm	thickness: 0.0002 mm
Total Device	-	area: 314.16 mm^2		

Note: The thickness of the barrier/walls is 10 times the thickness of the thermocouples and heater.

Table 2. Physical and electrical properties. Properties were provided by Kang, W. et al. (2018).

Thermocouple Material Properties			
Part	**Material**	**Property**	
Heater	**Evanohm R (Ni-Cr Alloy)**	Electrical Resistivity (@RT)	134.0 μΩ/cm
		Thermal conductivity	14.6 W/mK
		Density	8.11 g/cm^3
Thermocouple 1	**Chromel (Ni-Cr Alloy)**	Electrical Resistivity (@RT)	70.6 μΩ/cm
		Thermal conductivity	19.0 W/mK
		Seebeck Coefficient (@273K)	21.7 μV/K
		Density	8.50 g/cm^3
Thermocouple 2	**Constantan (Cu-Ni Alloy)**	Electrical Resistivity (@RT)	52.0 μΩ/cm
		Thermal conductivity	19.5 W/mK
		Seebeck Coefficient (@273K)	-35 μV/K
		Density	8.89 g/cm^3

Note: Heater electrical resistivity >> thermocouples electrical resistivity. We modified and used COMSOL's Bismuth Telluride, a material in the thermoelectric library. Using Bismuth Telluride and Lead Telluride may be a better option for higher sensitivity.

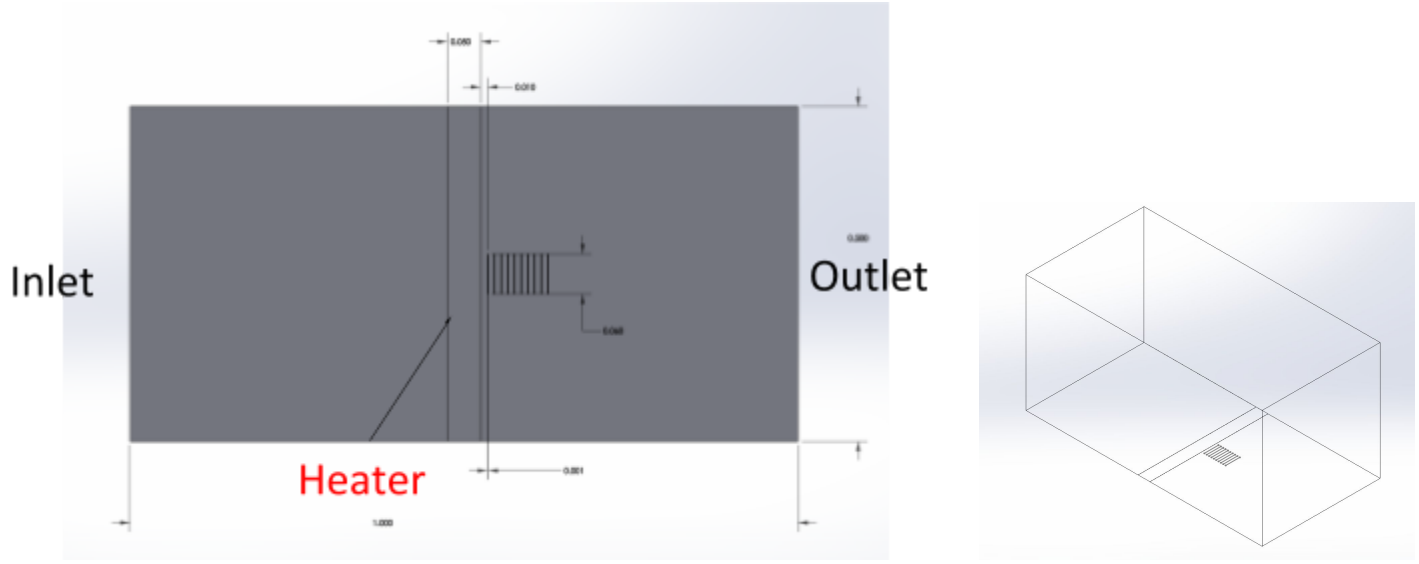

(a) Simple flow field model

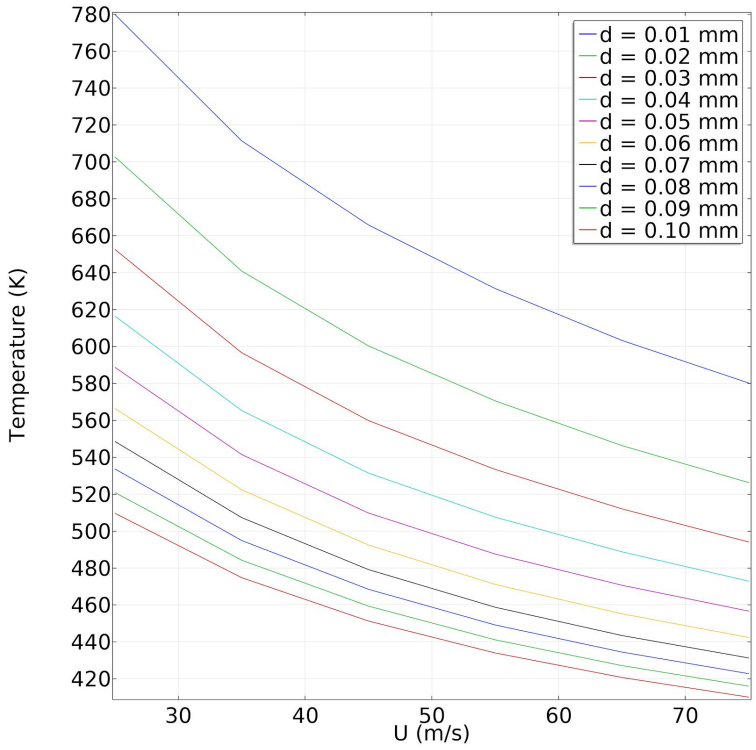

(b) Wind speed sweep simulation results

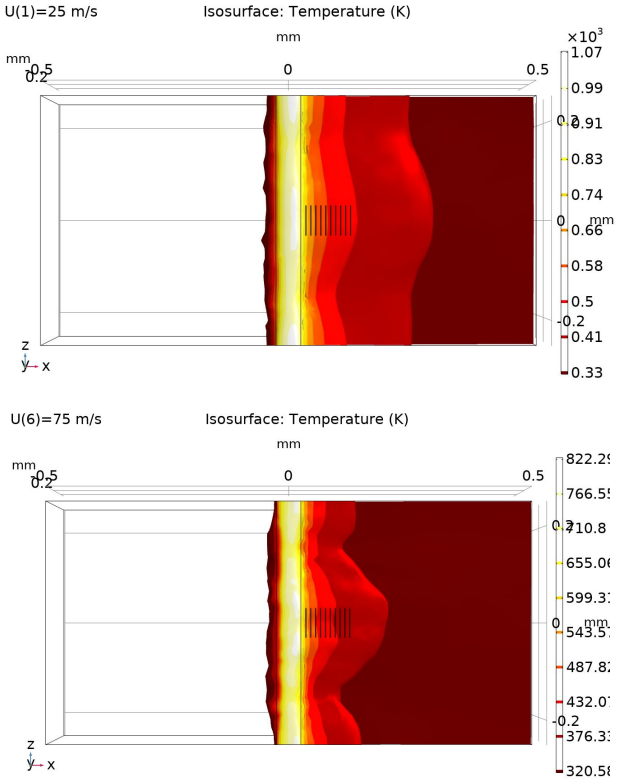

(c) Temperature isosurface gradient

Figure 3. Simple flow field model to demonstrate the effect at different gap distances. The model (a) was used to show how each distance is more or less sensitive at different speeds (b). Smaller gap distances have a steeper slope at high wind speeds. At a fixed power and low wind speeds, the temperature increases (c) because the wind has a cooling effect. Thus, the smaller gap distances are better for higher wind speeds.

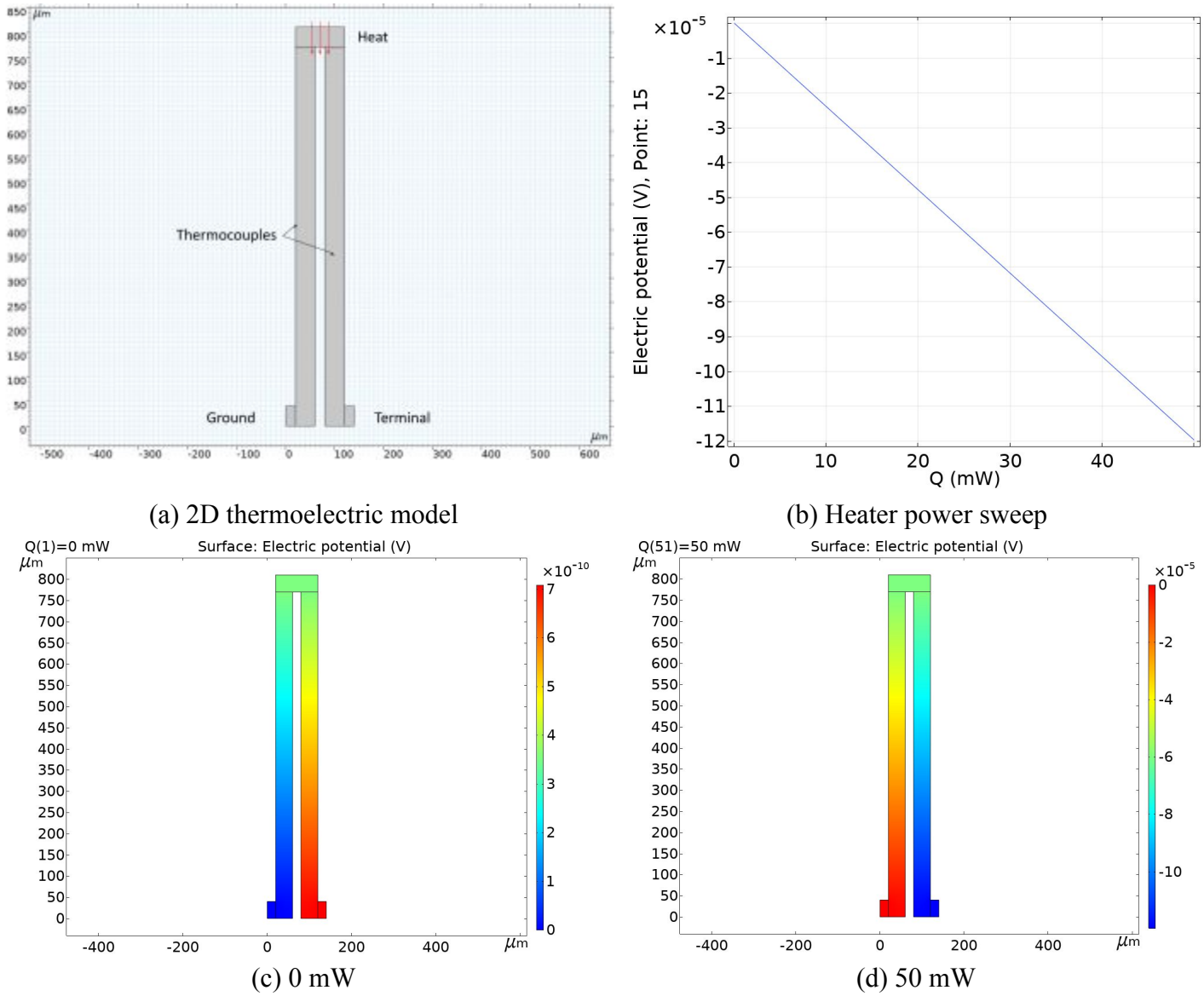

(a) 2D thermoelectric model

(b) Heater power sweep

(c) 0 mW

(d) 50 mW

Figure 4. Simple thermoelectric effect demonstration study. This model is used to demonstrate and test a COMSOL thermoelectric study. A simple 2D model (a) was utilized with a grounded end and a terminal end supplying a constant 0.001 mA of current. At the thermocouple tip, a heat source was added, and the heater power was swept from 0-50 mW. The results of the sweep (b) show that the electric potential difference across the ground and terminal change with the amount of heat, changing the electric potential by an order of magnitude of 10^5 as shown by the electric potential surface plots (c) and (d) at 0 mW and 50 mW, respectively.

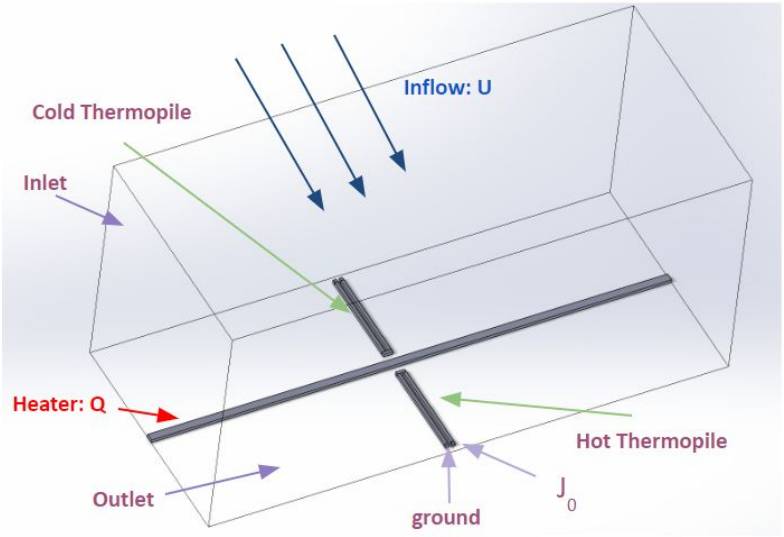

(a) Thermoelectric model

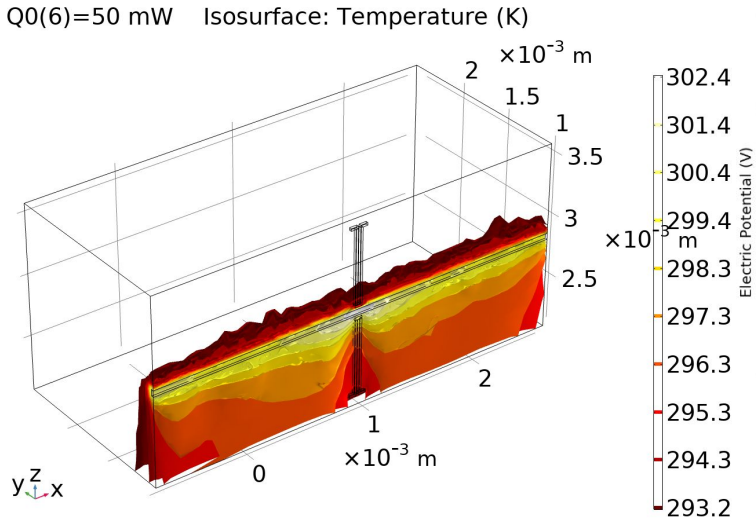

(b) COMSOL result

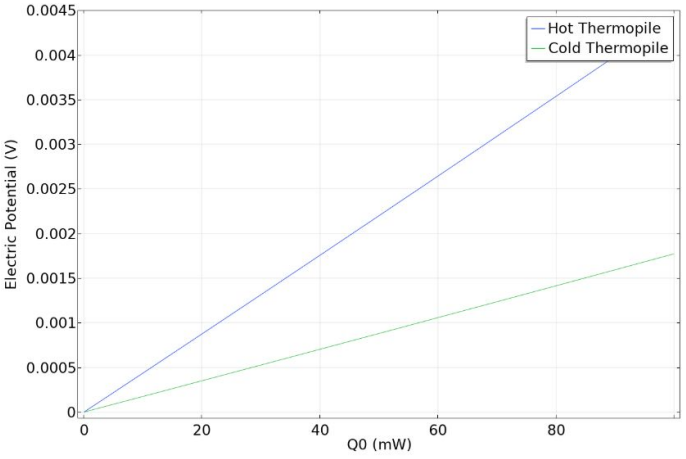

(c) Heater power sweep plot

Figure continues on next page.

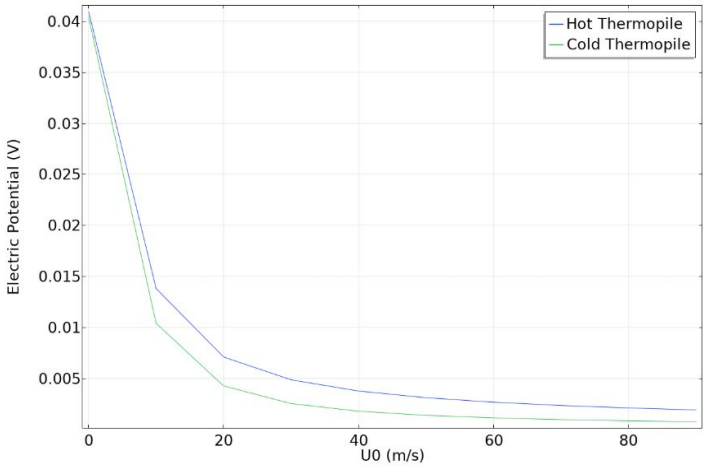

(d) Wind speed sweep plot

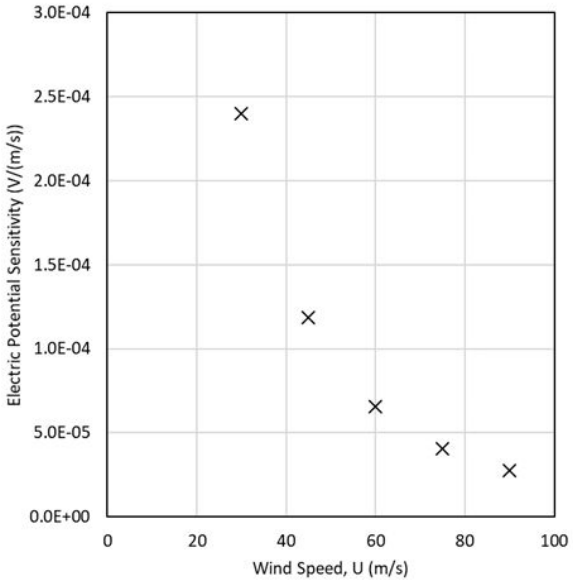

(e) Sensitivity of the thermoelectric model

Figure 5. Study of thermoelectric effect on a 20 μm model of the device. The structure of the thermoelectric model is shown in (a), the height of the heater and the thermopiles are 20 μm. Temperature isosurface contours of the one test result (b). The result of the Q sweep (c) shows that when heater power Q increases, the electric potential also increases. The result of the U sweep (d) shows the when flow rate increases, the electric potential decreases, and there is a linear and non-zero region at 75 m/s. Sensitivity of the model is the derivative of the function of the electric potential to flow rate (e). Because there is only one pair of thermocouples in this simulation, the sensitivity was multiplied by 37. The sensitivity at 75 m/s is 0.63 mV/(m/s), which is not sensitive enough.

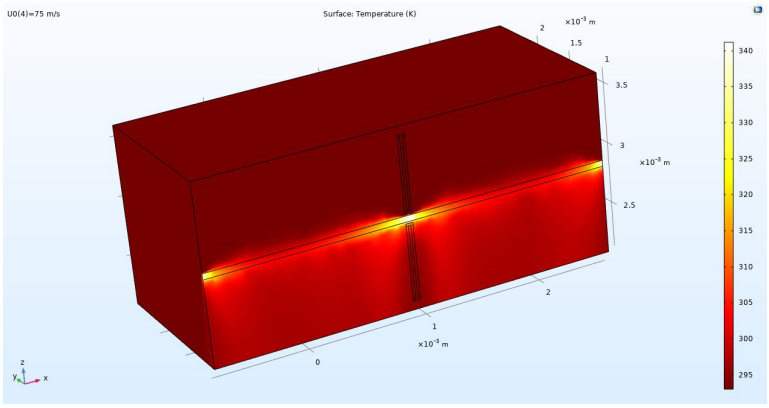

(a) COMSOL plot (Q0 = 50 mW; U = 75 m/s)

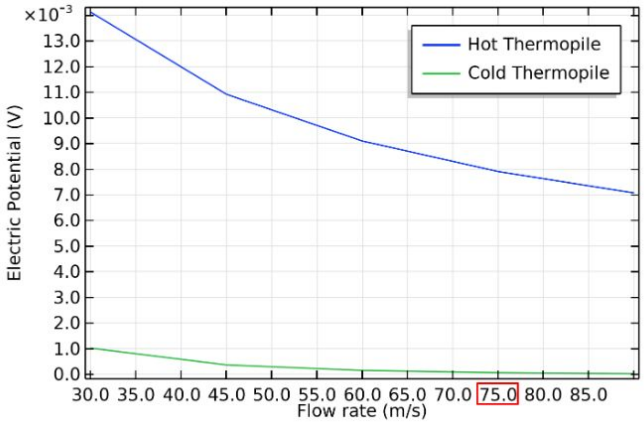

(b) Wind speed sweep plot of the real model

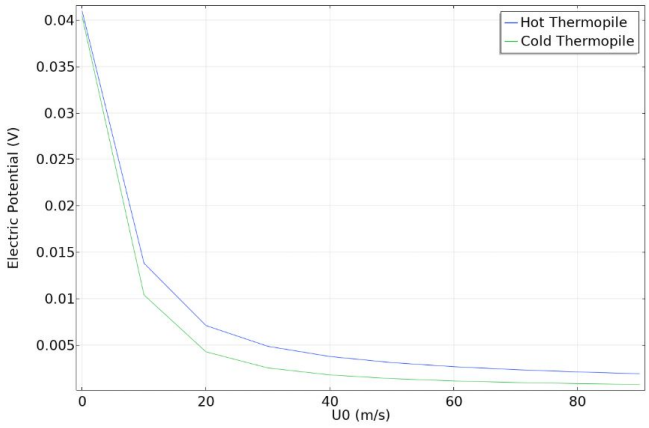

(c) Wind speed sweep of the thermoelectric model

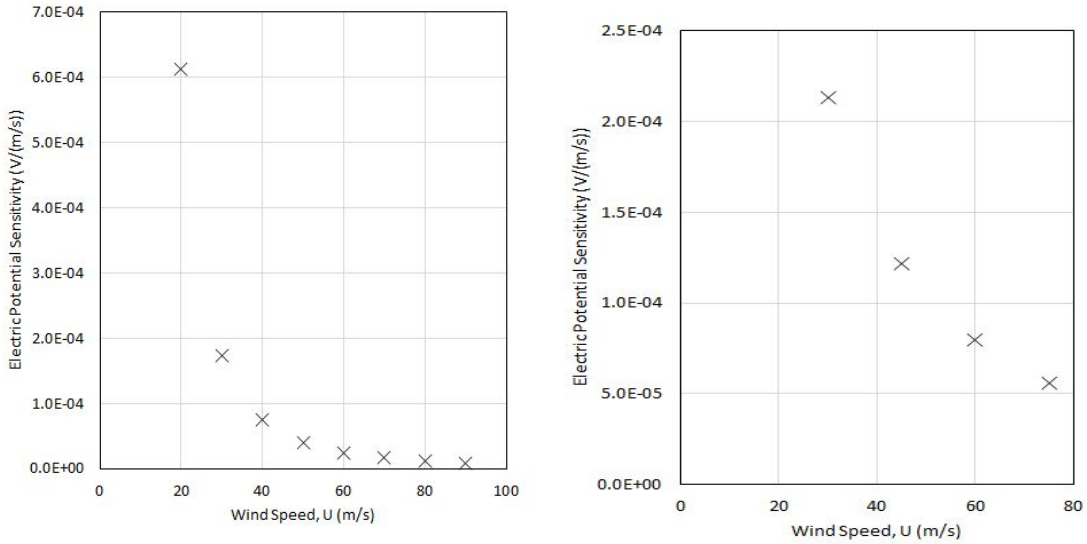

(d) Sensitivity comparison of thermoelectric model (left) versus real model (right)

Figure 6. In the real model, the height of the heater and the thermopiles are 200nm. The COMSOL result (a) shows the surface temperature contour at Q_0 = 50 mV and U = 75 m/s. Comparing (b) and (c), the slope of the hot thermopile of the real model at 75 m/s is larger than the thermoelectric model's. The sensitivity plot comparison (d) shows that the sensitivity of the real model is larger than the thermoelectric model's. Multiplying the sensitivity by 37, the sensitivity at 75 m/s is 2.06 mV/(m/s), which is sensitive enough.

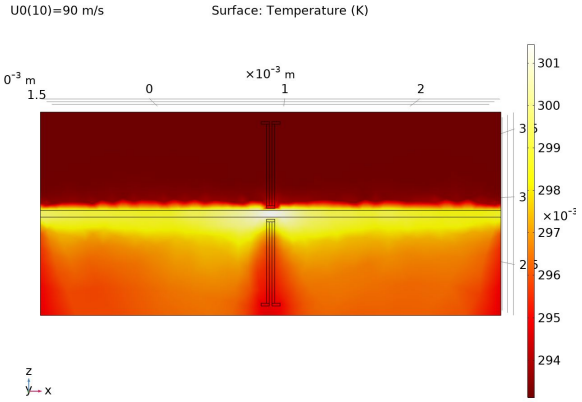

(a) 1 pair surface temperature

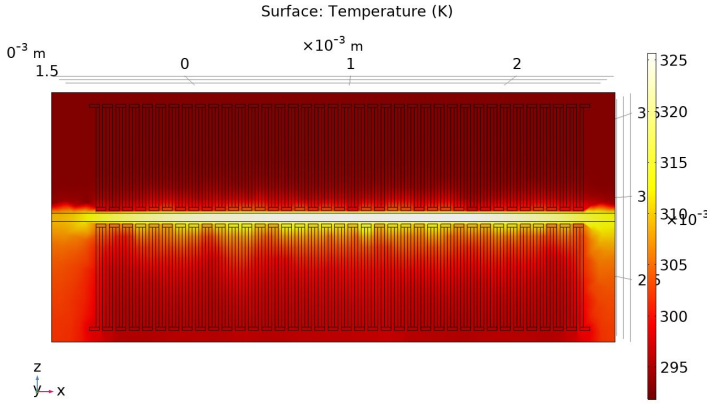

(b) 37 pair surface temperature

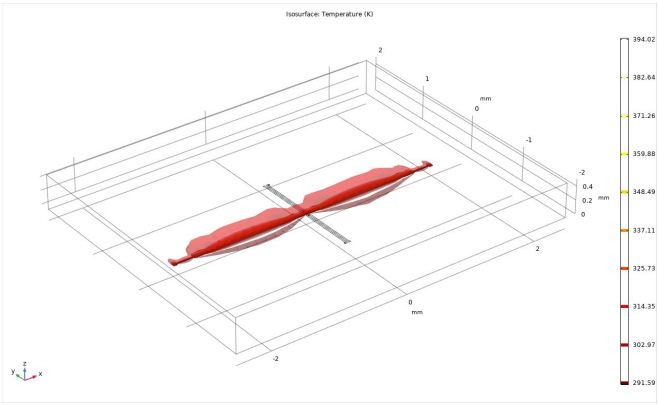

(c) 1 pair isosurface temperature contour

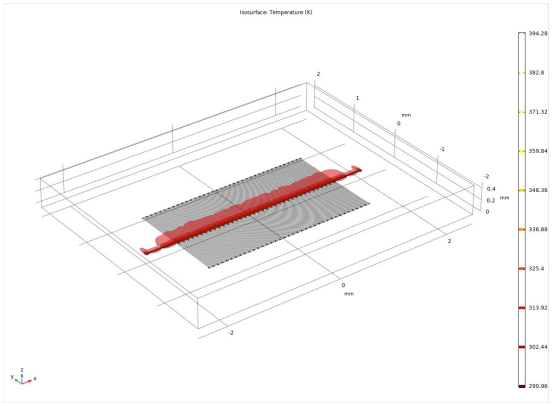

(d) 37 pair isosurface temperature contour

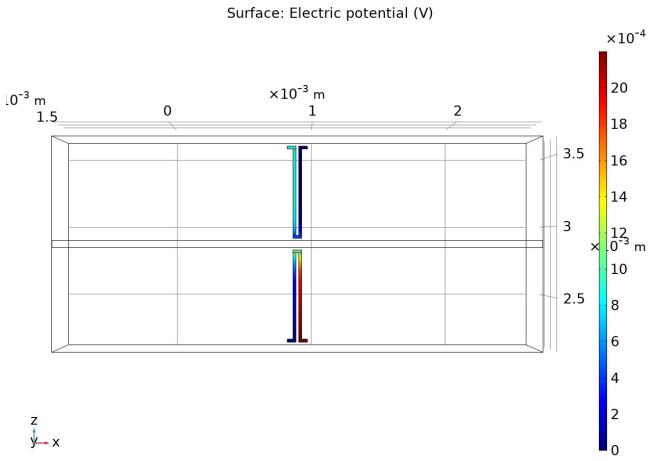

(e) 1 pair surface electric potential

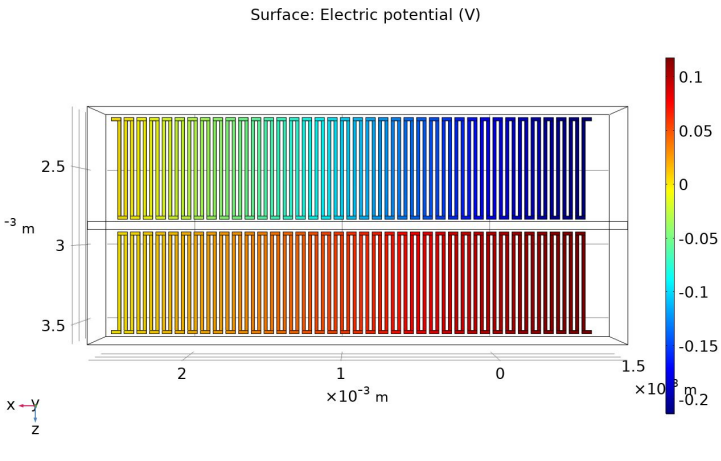

(f) 37 pair surface electric potential

Figure 7. Study of the effects of 1 pair and 37 pairs of thermocouples. Just from one pair of thermocouples, the flow is affected as shown by the temperature patterns in (a) and (c). The thermocouple geometry seems to have a heat trapping effect as there is a much higher temperature between the heater and the thermocouple. Having multiple seems to amplify this effect as shown by (b) and (d). The temperature reached is much greater than the 1 pair (301 K vs 325K). As a result of this heat trapping effect, the signal (electric potential) is amplified more than just by 37 as shown by the increase in the order of magnitude shown in (e) and (f) going from 10^{-4} to 10^{1}.